Material characterization of seven photovoltaic backsheets using seven accelerated test conditions

Soňa Uličná,[1,2] Rachael L. Arnold,[2] Jimmy M. Newkirk,[2] Archana Sinha,[1] Kent Terwilliger,[2] Laura T. Schelhas,[2] Peter Pasmans,[3] Christopher Thellen,[4] David C. Miller[2]

[1]SLAC National Accelerator Laboratory, Menlo Park, CA 94025, USA

[2]National Renewable Energy Laboratory, Golden, CO 80401, USA

[3]Endurans Solar, Urmond, 6129 EL, The Netherlands

[4]Endurans Solar, Nashua, NH 03063, USA

Abstract:

A variety of polymeric backsheet materials can be found in fielded photovoltaic (PV) modules, mostly based on fluoropolymer and polyethylene terephthalate (PET) materials. Cost reduction and sustainability considerations drive the recent development of alternative backsheet materials and designs [1]. In some fielded PV installations, polymeric materials are susceptible to environmental degradation in the form of backsheet cracking. To prevent backsheet degradation that can result in a module failure, thorough laboratory reliability testing is needed. Here, we studied the durability of seven commercial and experimental PV backsheets through accelerated stress testing using seven photolytic, hygrometric, and custom tests with the goal to understand if novel fluoropolymer-free backsheets are sufficiently environmentally durable to be commercialized. We divided the mechanisms observed during aging into two categories: core degradation and surface degradation. Although core degradation due to hydrolysis was observed in all commercial PET-, and polyamide (PA)-based backsheets aged with 85°C/85% relative humidity, this test is unlikely to be field relevant. Photo-oxidative reactions on the exposed surface during UV weathering affected all seven backsheets regardless of the outer layer polymer material and additives. This degradation was limited to the outermost micrometers of the surface, except for backsheets containing PA-12, which resulted in surface cracking. A custom test combining UV with water spray caused the most severe backsheet degradation, including surface erosion and loss of insulating properties in polyolefin (PO)- and PA-based backsheets. This highlights the importance of combined accelerated stress testing to screen for complex backsheet degradation mechanisms. We also showed that, with material and design optimization, coextruded experimental PO-based backsheets have the potential to be a durable alternative to commercial PET- and fluoropolymer-based PV backsheets.

Keywords:

BACKFLIP, backsheet, damp heat testing, durability, DuraMAT, IEC TS 62788-7-2, PET, polyamide, polyolefin, UV weathering

1/ Introduction

The role of polymeric photovoltaic (PV) backsheets is to protect the inner cell matrix from environmental impacts and provide a proper electrical insulation from high operational voltages throughout the module warranted period of 25 to 30 years. As the PV module industry rapidly expands, there is a growing interest in replacing the benchmark polymeric backsheets with cheaper and more recyclable alternatives while maintaining high material reliability relative to the life span of PV modules. Traditional PV backsheets are typically three-structural-layered laminates consisting of weather-durable fluoropolymer outer layers, such as polyvinyl fluoride (PVF), and a mechanically robust and insulating polyethylene terephthalate (PET) core. Each layer has a unique additive and stabilizing formulation and is specific to the backsheet manufacturer. TPT (PVF/PET/PVF) backsheets have been used in PV module installations since the 1980s and have been proven to have great field reliability, with few adverse incidents over the past 30+ years. However, fluoropolymers are relatively expensive, presently in short supply [1], and there are concerns over their safety and recyclability, in addition to the release of toxic gases in the event of overheating [2],[3]. Alternative materials, such as polyolefins (POs) and polyamides (PAs), have entered the PV backsheet market in recent years as competitors to fluoropolymers. In addition of being more sustainable [3], these emerging backsheets are produced by coextrusion, which simplifies the manufacturing process, reduces costs as well as risks of interlayer delamination by eliminating glue [1]. However, catastrophic, wide-spread premature field failures of the PA-based backsheet AAA serve as a reminder that thorough and relevant testing is required prior to the large-scale deployment of new backsheets [4].

In this systematic study, we evaluated the durability of PV backsheets by comparing seven commercial and emerging fluoropolymer-free PV backsheets through seven accelerated test conditions using ultraviolet (UV), damp heat, elevated temperature, and water spray environmental stimuli. An independent assessment of the durability of recently developed backsheets was performed relative to past and present backsheet products. A previous publication summarized the impacts of these same backsheets on module performance through current-voltage measurements and electroluminescence imaging [5]. The artificial weathering in this study will be separately compared to natural weathering at two geographical locations with different climates to validate that the applied tests are field relevant. In the Köppen-Geiger climate system [6], the two locations in the separate outdoor study described in Ref. [7] include a warm-dry steppe climate (BSk) in Albuquerque, New Mexico, U.S.A. and a warm-humid sub-tropical climate (Cfa) in Cocoa, Florida, U.S.A. The work presented here focuses on changes in the material properties of the different types of backsheets during the accelerated stress tests to evaluate their long-term durability. We divided the seven backsheets into three groups based on their core material (i.e., PET, PA, and PO), identified using differential scanning calorimetry (DSC) and wide-angle X-ray scattering (WAXS) [8]. Photolytic, hygrometric, and custom aging tests combining UV and water spray showed material-specific degradation mechanisms, including UV-induced photo-oxidation and hydrolytic degradation, resulting in surface erosion and cracking from embrittlement. Changes in material properties were correlated with changes in mechanical characteristics using tensile testing. This work compared the degradation of legacy backsheets to that of materials that are entering the market and need to be validated to avoid catastrophic failures, as in Ref. [4]. While degradation of commercial backsheets was dominated by bulk degradation of the PET core in hot and humid conditions, emerging fluoropolymer-free backsheets were susceptible to surface damage from UV photo-oxidation, with the backsheet core largely unaffected. This study demonstrates that emerging fluoropolymer-free backsheets can be robust and durable, which is promising for the PV backsheet industry.

2/ Materials and Methods:

a) Test specimens

The seven types of backsheets used in this study are described in Table I. The backsheet set includes benchmark and contemporary products (BS-3: TPT, BS-5: PPE, and BS-7: KPf), experimental products (BS-1: PO-1, BS-2: PO-2, and BS-4: APO), and one environmentally vulnerable product (BS-6: AAA). A table of all the acronyms is included as Table S1 in the Supplemental Information (SI). The backsheets were sourced from five unidentified manufacturers, with BS-3 (TPT), BS-5 (PPE), BS-6 (AAA), and BS-7 (KPf) being commercial products present in fielded PV installations. Backsheets were aged and characterized in the form of stand-alone backsheet coupons and backsheet/poly(ethylene-co-vinyl acetate) (EVA) laminated coupons with dimensions 17 cm x 17 cm. These were compared to backsheets aged in the form of mini modules (MiMos), also 17 cm x 17 cm. Fig. S1 in the SI shows photographs of backsheet coupons and MiMos. More information on the samples and their preparation can be found in related publications [5], [9].

Table I: Summary and description of studied backsheets.

Material Group	Arb. Index	Backsheet Name	Composition	Comments	Manufacturer
PO-based	BS-1	PO-1	PO/PO/LDPE	In development	a
	BS-2	PO-2	PBT/PO/LDPE	In development	a
	BS-4	APO	PA/PO/LDPE	Recently developed	a
PA-based	BS-6	AAA	PA/PP-PA/PA	Environmentally vulnerable	b
PET-based	BS-3	TPT	PVF/PET/PVF	Benchmark	c
	BS-5	PPE	PET/PET/LDPE	Contemporary	d
	BS-7	KPf	PVDF/PET/F-coating	Contemporary	e

b) Accelerated stress tests

Coupons and MiMos were aged using the accelerated test conditions described in Table II. Test conditions a (A3), d (A2), and 1 (85°C/85% relative humidity (RH)) are based on International Electrochemical Commission (IEC) standards [10],[11]. The other hygrometric tests—2 (65°C/85% RH) and 3 (45°C/85% RH)—are similar to 1 (85°C/85% RH), but use lower chamber temperatures. Custom test b is based on the backsheet manufacturer's methods and includes UV with lower intensity than the IEC methods (A2 and A3). Custom test c applies the same UV intensity as custom test b, in addition to water spray (in the form of fine water mist). We performed material analysis of the coupons at intermediate read points at 0, 1000, 2000, 3000, and 4000 h of weathering. At each read point, one of four identical coupons was retrieved without replacement and subsequently diced into replicate specimens (e.g., Weibull analysis) for various characterizations as shown in Ref. [9]. Aging and characterization of backsheet coupons is schematically represented in the flow chart in Fig. S2. Destructive characterization of the MiMos was performed at the end of weathering (4000 h). Accelerated weathering with IEC TS 62788-7-2 methods a (A3) and d (A2) [10] and custom weathering (tests b and c) were performed using xenon lamp chambers (Ci5000 Weather-Ometer, Atlas Material Testing Technology, LLC). Hygrometric aging was performed in damp heat chambers (BTX-475, ESPEC North America, Inc.). Coupons and MiMo

specimens were mounted in the chambers with the air side facing the xenon lamp and water spray in corresponding tests.

Table II: Summary of accelerated stress tests.

Test Type	Test Index	UV Irradiance ($W \cdot m^{-2}$ at 340 nm)	Chamber Temperature (°C)	Chamber Relative Humidity (%)	Water Spray?
Photolytic	a (A3)	0.8	65	20	N
	d (A2)	0.8	55	20	N
Hygrometric	1	0	85	85	N
	2	0	65	85	N
	3	0	45	85	N
Custom	b	0.55	60	20	N
	c	0.55	60	~80	Y

c) Characterization

Backsheet samples were analyzed using the below-described morphological, structural, chemical, and mechanical characterization techniques. In laminated PET-based backsheets, the individual backsheet layers can be separated and studied individually by dissolving the interlayer adhesive in acetone [12]. The layers of coextruded PA- and PO-based backsheets cannot be easily separated, and therefore these backsheets were only examined as a whole.

DSC was performed using a TA Instruments Q2000 differential scanning calorimeter equipped with an RCS 90 refrigerating unit to measure thermal transitions of various polymers in the backsheet layers. Circular samples weighing approximately 7—12 mg were prepared in a non-hermetic aluminum pan and subjected to a heat-cool-heat cycle at a rate of 10°C/min, while constantly purged with N_2 gas at a rate of 50 mL/min.

To rapidly evaluate the crystal structure of the many specimens in this study, WAXS data were collected at beamline 11-3, at the Stanford Synchrotron Radiation Lightsource (SSRL) user facility at SLAC National Accelerator Laboratory. Rectangular backsheet samples were placed in transmission geometry at a distance of 200 mm from the charge coupled device (CCD) area detector (Rayonix MX225) with the backsheet air side facing the detector. Samples were exposed to 12.7-keV X-rays for 30 s. The WAXS data were calibrated using a lanthanum hexaboride (LaB_6) standard and analyzed using the General Structure and Analysis Software (GSAS-II) [13]. The 2D scattering patterns were integrated and plotted as a function of a scattering vector, $Q = \frac{4\pi}{\lambda}\sin\left(\frac{2\theta}{2}\right)$.

The backsheet polymer surface chemistry was examined using an ALPHA-II spectrometer from Bruker Corp. in attenuated total reflection (ATR) mode. Fourier transform infrared (FTIR) spectra on each side (air side, sun side) of the backsheets were measured using a single reflection diamond ATR crystal fixture from Bruker Corp. with a sampling depth of ~2 µm. Measurements were taken from the average of 50 scans, from 4000 to 400 cm^{-1}, using a 2 cm^{-1} increment. Two measurements per backsheet side were taken to verify valid measurement. Data was normalized to the carbon-hydrogen (C-H) vibration at 1410 cm^{-1} that is common to all backsheets.

High-resolution thermogravimetric analysis (TGA) of the backsheet coupons was performed using a Discovery TGA 5500 (TA Instruments). Circular samples were heated in platinum pans between 40°C and 700°C at a heating rate of 20°C/min, which was reduced to 4°C/min during weight loss events.

Visual appearance of the backsheet surface was photographed using an α99 MII digital camera (Sony Corp.), and surface microstructure was imaged using a VHX-5000 digital microscope (Keyence Corp.).

Mechanical tensile tests were conducted on five strips, each 15 cm long x 1 cm wide, cut from each coupon sample to identify changes in overall mechanical integrity. Tensile test was developed in the IEC 62788-2 standard [14] in response to the embrittlement and cracking observed in AAA backsheets. The longer dimension of each strip was aligned with the transverse direction of the backsheet extrusion. All specimens were loaded with a 10-mm gage region, except BS-6 (AAA) with a 50-mm gage length. Tests were performed at a crosshead displacement of 50 mm/min and a data acquisition rate of 500 Hz using a Tensile Tester (Instron Corp.) with the Automatic Video Extensometer attachment and a 5–10-kN load cell.

Dielectric breakdown voltage (V_{BD}) testing of the backsheet was performed to verify electrical insulation according to IEC 61730-2 [15], using a 4TCE100-10/D149 tester (Phenix Technologies Inc.) in Univolt N61 transformer oil. The DC voltage was applied between 25-mm-diameter brass electrodes at a ramp rate of 5 kVs^{-1}, and the current was limited to 10 mA. Six pre-conditioned 50-mm x 45-mm replicate specimens were tested with a positive terminal connected to the air side of the backsheet. Weibull analysis was performed to analyze data from replicate samples from tensile testing and V_{BD}.

Further details on the characterization used here as well as other methods, including color, gloss, and fractography, can be found in Ref. [9].

3/ Results: Degradation mechanisms in backsheets

Backsheets' core material is either PET (benchmark and contemporary laminated backsheets), PA (environmentally vulnerable AAA), or PO (experimental, coextruded backsheets). The core layer dominates the mechanical properties of the backsheet (tensile strength and elongation to break), as was shown in Ref. [5]. Backsheet durability depends on both the core layer material and the ability of the outer layer to protect it from the environment. The following subsections will describe differences in degradation mechanisms observed in the three groups of backsheets.

a) Benchmark and contemporary PET-based laminated backsheets

Industry-benchmark backsheets BS-3 (TPT), BS-5 (PPE), and BS-7 (KPf) have a laminated structure containing a PET core layer but different protective outer (air side) and adhesive inner (sun side) layers. WAXS and DSC confirm that the air and sun side layers in BS-3 (TPT) are both PVF. In BS-5 (PPE), they are PET and low-density polyethylene (LDPE), respectively, and in BS-7 (KPf), they are polyvinylidene fluoride (PVDF) and fluorinated coating, respectively. A thin fluorine coating intends to address the UV protection on the cell side while being less expensive than a fluoropolymer film such as PVDF [1]. Fig. 1 shows DSC thermograms of backsheet coupons from BS-5 (PPE) and BS-7 (KPf), comparing accelerated tests 1 (85°C/85% RH), a (A3), b (custom, UV), and c (UV and water spray) to the unaged specimen.

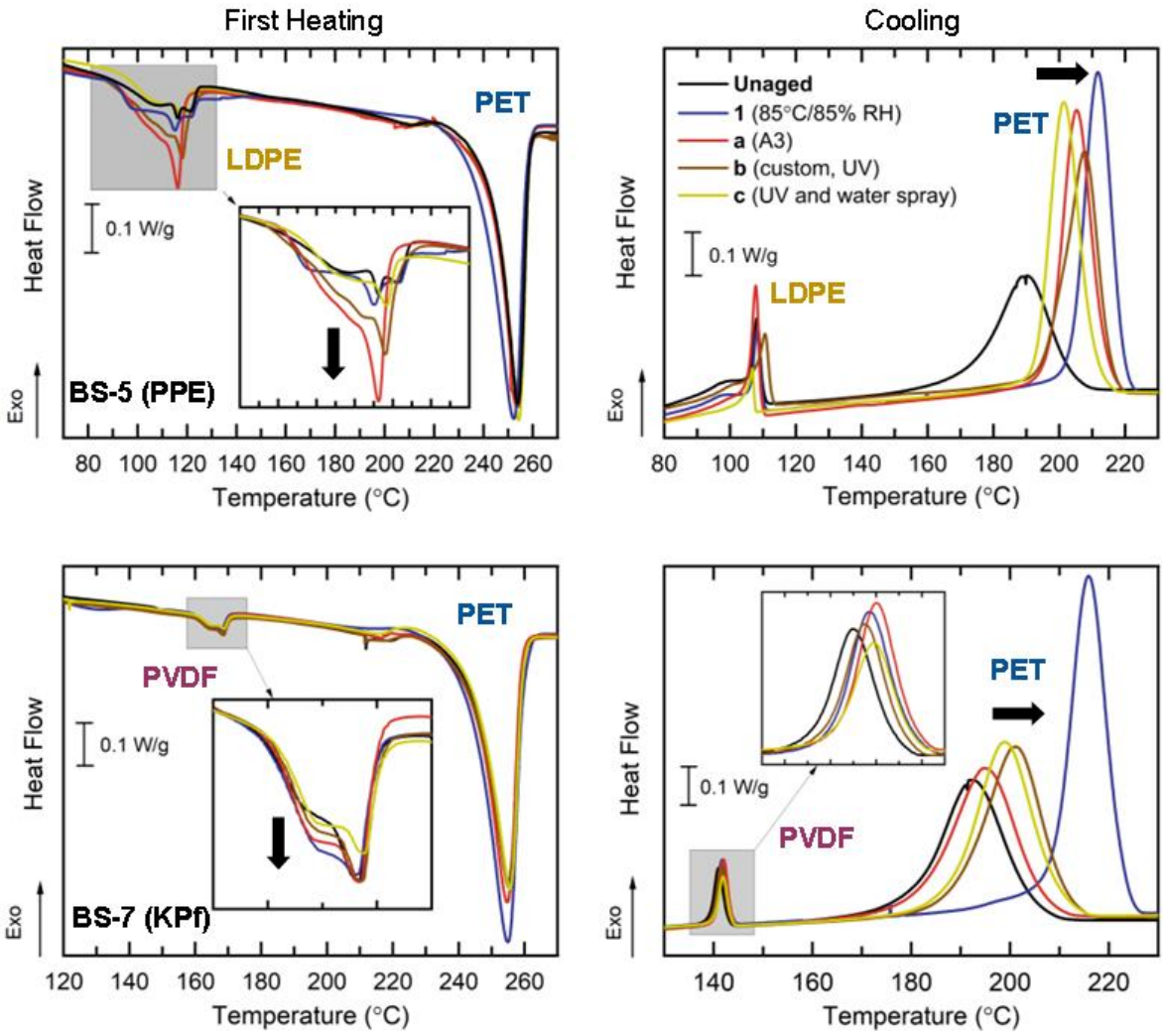

Fig. 1 DSC thermograms from the first heating cycle (left) and cooling cycle (right) of PET-based backsheets BS-5 (PPE) and BS-7 (KPf) after 4000 h of aging with various tests. Arrows indicate important material changes, including an increase in crystallinity (vertical arrow) in the first heating and changes in molecular weight (horizontal arrow) in the cooling cycles.

DSC thermograms show peaks corresponding to melting (first heating cycle) and crystallization (cooling cycle) of different materials in the backsheet. The lower-temperature smaller-intensity peaks identify the thin sun side (LDPE in BS-5 (PPE)) and air side (PVDF in BS-7 (KPf)) backsheet layers, whereas the more prominent high-temperature peaks at 255°C identify the PET in the core (BS-7 (KPf)) or PET core and air side layers (BS-5 (PPE)). The PET crystallization peak increased in intensity and rose by over 20°C for all PET-based backsheets aged by test condition 1 (85°C/85% RH). This shift is caused by hydrolysis-induced chain scission of the polymer backbone. Hydrolysis of PET is a well-known degradation mode affecting PET polymers, where under hot and humid conditions, the ester functional group degrades to form carbonyl- and hydroxyl-terminated end groups and smaller chain fragments [16]. Fig. 2 shows DSC of BS-3 (TPT) for 85% RH and temperatures 85°C, 65°C, and 45°C (tests 1, 2, and 3, respectively). Negligible changes in DSC are observed for the two lowest temperatures, but progressive shifts to higher

temperatures of the PET crystallization peak during aging with test condition 1 (85°C/85% RH) are observed. The temperature of 85°C is above the glass transition temperature (T_g) of PET (80°C), where the chain mobility is increased and the polymer is in the rubbery state [17],[18]. The chain scission is accompanied by an increase in crystallinity, indicated by an increase in the area under the melting peak (Fig. 1 and Fig. 2). The chain scission occurs in the amorphous phase of PET, leaving disentangled chain segments able to crystallize [19]. The damage to the core during test 1 (85°C/85% RH) suggests that the outer protective layers were not able to protect the core from the effects of hydrolytic aging (backsheets are typically permeable to water and oxygen). Test 1 (85°C/85% RH) resulted in significant embrittlement and complete loss of integrity of the PET core, compromising the entire backsheet. Consequently, no tensile test data could be obtained, and cutting the backsheet from the aged MiMos resulted in crumbling of the PET layers. Damp heat 85°C/85% RH is, however, considered greatly accelerated and not representative of real-world outdoor operational conditions [20].

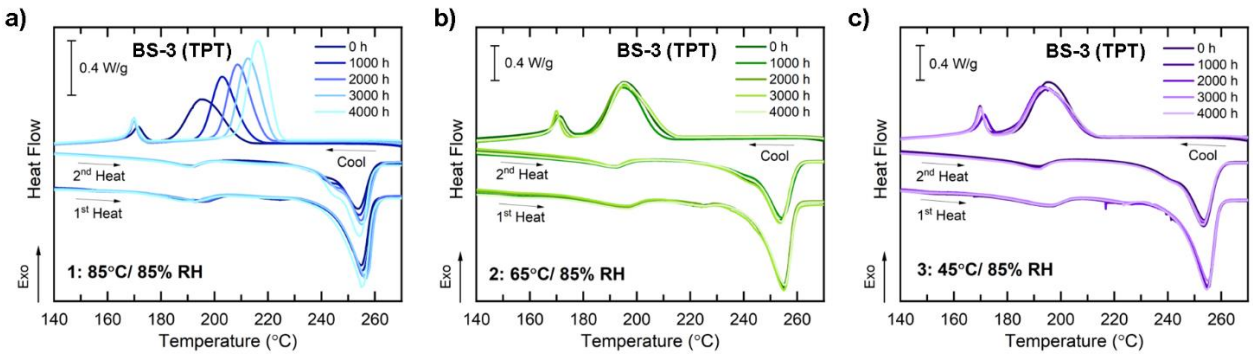

Fig. 2 DSC of PET-based BS-3 (TPT) at various read points during hygrometric aging with three different temperatures: (a) test 1: 85°C/85% RH, (b) test 2: 65°C/85% RH, and (c) test 3: 45°C/85% RH.

UV weathering tests a (A3), b (custom, UV), c (UV and water spray), and d (A2) also resulted in PET chain scission from UV photo-oxidation reactions of Norrish type I and type II [16],[21]. Photolytic aging forms volatile CO and CO_2 products and -COOH (terephthalic acid) end functionalities at the surface of the film. The increase in temperature of the PET crystallization peak in the DSC of BS-5 (PPE) after photolytic and custom tests suggests UV photo-oxidative degradation of the air side PET layer (Fig. 1). The FTIR data from the outer (air side) PET surface in Fig. S3 shows an increase in hydroxyl (-OH ~ 3000 cm^{-1}) and carbonyl (C=O ~ 1700 cm^{-1}) functional groups in all four UV tests, but negligible changes after either of the three hygrometric tests. The air side layer is typically formulated with stabilizers and antioxidants intended to reduce the photo-oxidative degradation. As such, this UV-induced degradation was limited to the backsheet outer surface, and the core layer was not affected by UV tests, as shown in the DSC of the core layer separated from the other backsheet layers (Fig. S4).

UV weathering also resulted in significant structural and chemical changes to the air side fluoropolymer PVF and PVDF layers. Fig. 3 shows changes in the outer (air side) PVF layer through test a (A3), which is generally representative of all photolytic (including custom) test conditions (a, b, c, and d). The TGA weight loss curves indicate that after only 1000 h of UV weathering, the decomposition temperature of PVF dropped from 300°C to 250°C (Fig. 3a). The FTIR spectra confirm oxidation of the polymer backbone and additives—evidenced by an increase in the peaks corresponding to carbonyl (C=O)

and C-O functional groups at 1730 cm^{-1} and 1200 cm^{-1}, respectively (Fig. 3b). DSC (Fig. 2) and WAXS diffractograms (Fig. 3c) show changes in crystal structure and preferred crystal orientation of the semicrystalline polymer from aging. No surface micro-scale changes were observed with the optical microscope after UV weathering (Fig. 3d) or hygrometric aging [9].

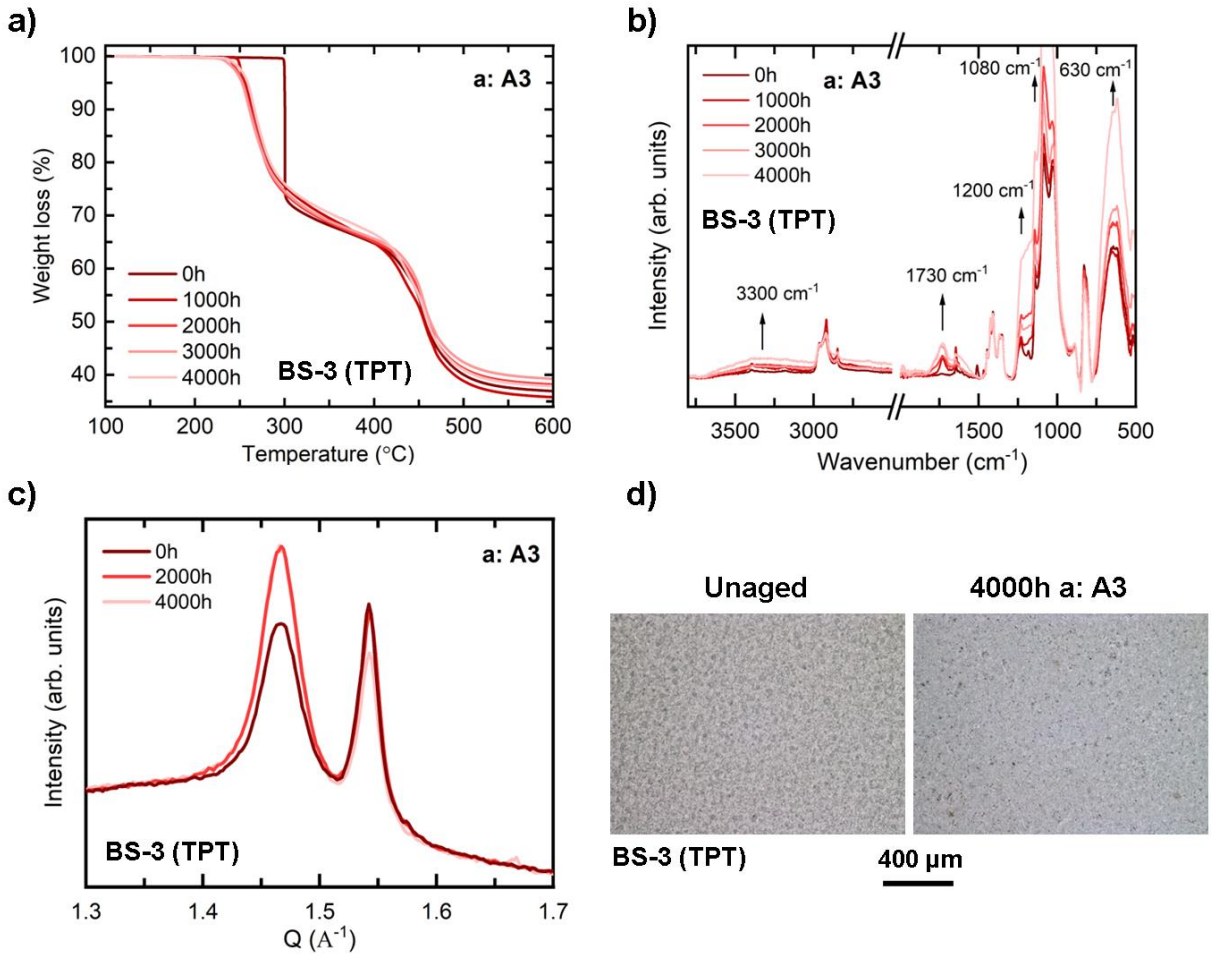

Fig. 3 Analysis of PVF air side layer in BS-3 (TPT) through UV weathering (test a, IEC method A3): (a) TGA decomposition profiles, (b) FTIR-ATR spectra of the UV-exposed air side surface, (c) WAXS diffractograms, and (d) optical microscope images of the surface.

Degradation of PVDF-based backsheets was recently studied because of premature field cracking [22]. Degradation mechanisms include an increase in crystallinity, depletion of the acrylic co-polymer, and crystalline phase change [23],[24]. Although no micro- or macro-cracking was observed in any of the coupon or MiMo specimens in this study [9], the degradation mechanisms detected here are the same as in the literature. Polymethyl methacrylate (PMMA) depletion, evidenced by a decrease of the carbonyl functional group at 1730 cm^{-1} in the FTIR spectra (Fig. S5a) and an increase in crystallinity observed in DSC first heating (Fig. S5b), were present for all UV weathering and hygrometric test conditions, where degradation was enhanced with increasing chamber temperature and UV dose. Surface roughening

exposing titania pigment was deduced for test c (UV and water spray) from changes in the 800—500-cm^{-1} region of the FTIR spectra (Fig. S5a).

An increase in crystallinity causing cracking of the LDPE sun side layer of BS-5 (PPE) was observed for UV weathering. The inset of the first DSC heating curve in Fig. 1 shows a significant increase in peak area after UV weathering with test b (custom, UV intensity of 0.55 Wm^{-2}) and an even greater increase after UV weathering with test a (A3, UV intensity of 0.8 Wm^{-2}). The FTIR spectra in Fig. 4a show an increase in oxygen-containing functional groups (C-O at 1400—1000 cm^{-1} and C=O at 1710 cm^{-1}), confirming photo-oxidative degradation of the LDPE [25],[26]. All UV tests resulted in biaxial cracking of the sun side layer in aged coupons (with and without the UV-blocking encapsulant present) starting at 1000 h; however, no cracking was observed in MiMos. This result indicates that this degradation mechanism may not be relevant in modules where the backsheet sun side layer's role is to provide adhesion to the encapsulant and this layer will be shielded from UV by module components or UV-absorbing additives in the encapsulant. Test c resulted in the loss of material by erosion due to water spray. Fig. 4b shows visual images after 4000 h of UV weathering in test a (A3).

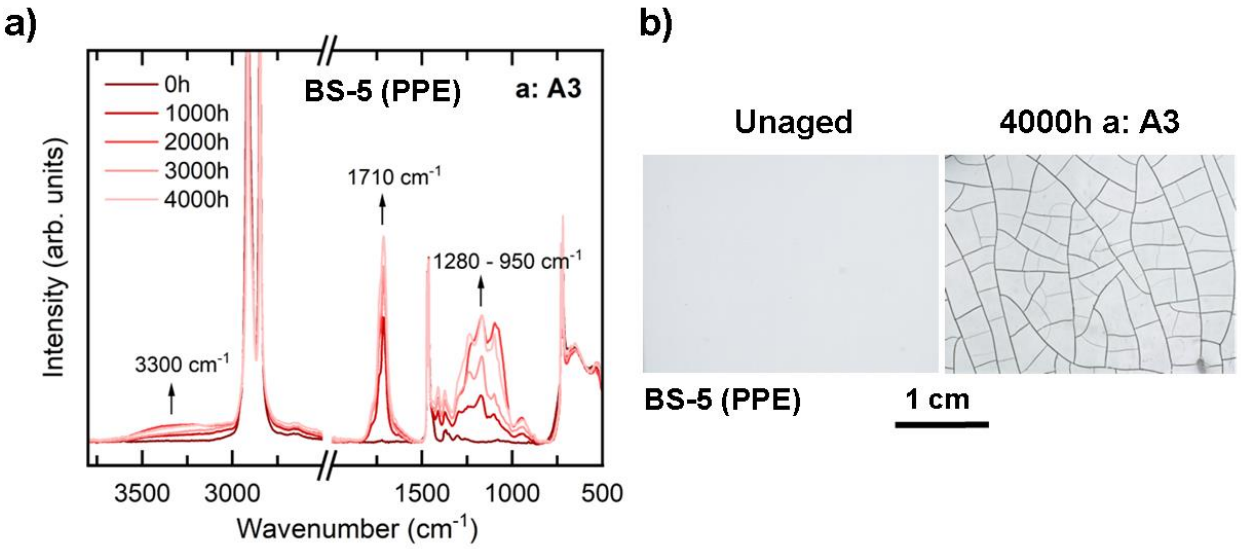

Fig. 4 (a) FTIR-ATR spectra of LDPE sun side layer in BS-5 (PPE) after test a (IEC method A3), representative of all photolytic tests, and (b) mud cracking of the LDPE sun side layer in stand-alone coupons (unencapsulated) of BS-5 (PPE) after test a (A3).

b) Polyamide-based backsheets

Polyamide-based BS-6 (AAA) is an environmentally vulnerable backsheet with field life of a few years rather than 30 years as in contemporary PV modules. It has been the subject of many degradation studies in recent years because of catastrophic premature field failures in the form of overt cracking, which exposes the module components [4]. AAA contains PA-12 in all three layers; however, the core is a blend of PA-12, polypropylene (PP), and glass fibers. Other studies have shown that PA-based backsheets should not all be considered environmentally vulnerable; it is the wrong design, choice of materials, and

manufacturing of the AAA that lead to failure [27],[28]. This section compares BS-6 (AAA) to a recently developed BS-4 (APO) that also contains PP and PA-12 to demonstrate the importance of the backsheet structure and design for its durability.

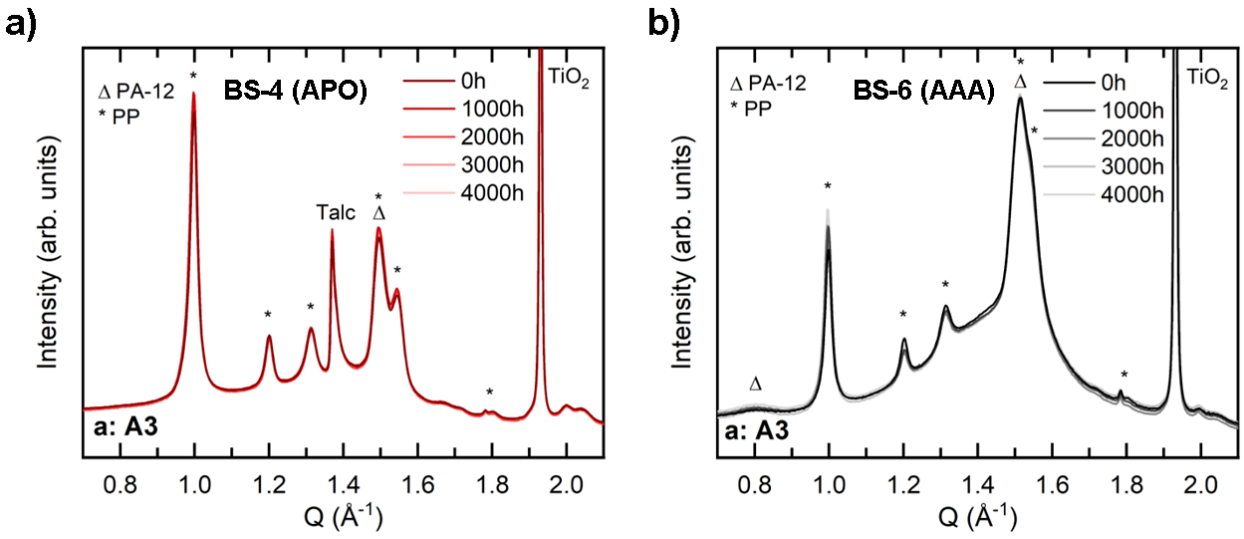

Fig. 5 WAXS diffractograms of (a) BS-4 (APO) and (b) BS-6 (AAA) aged for up to 4000 h with test a (A3).

WAXS (Fig. 5) and DSC (Fig. 6) techniques identified and confirmed PP and PA-12 to be the main materials present in both BS-4 (APO) and BS-6 (AAA). PP has a melting temperature (T_m) of 165°C and is represented by the scattering peaks and corresponding crystalline planes in Fig. 5 at Q = 1.0 $Å^{-1}$ (110), Q = 1.22 $Å^{-1}$ (040), Q = 1.33 $Å^{-1}$ (130), Q = 1.5 $Å^{-1}$ (131), Q = 1.58 $Å^{-1}$ (111), and Q = 1.8 $Å^{-1}$ (041). PA-12 melts at ~178°C, and the diffraction peak of its gamma phase overlaps with PP at Q = 1.5 $Å^{-1}$ (001), with a weak peak at Q = 0.8 $Å^{-1}$ (040). These are clearly distinguished only in BS-6 (AAA), as PA is the main material in all three layers of this backsheet. Both backsheets contain TiO_2 identified by a sharp peak at Q = 1.92 $Å^{-1}$, and BS-4 (APO) also contains talc mineral filler (Q = 1.4 $Å^{-1}$). The white TiO_2 pigment is often used as an additive in backsheet outer layers to improve the UV durability [29]. Instead of the glass fibers used in BS-6 (AAA), some coextruded backsheets including BS-4 (APO) use talc to improve the dimensional stability [27]. The backsheet layers cannot be separated in a coextruded backsheet and therefore cannot be studied separately. Despite the two backsheets having the same polymer materials, the differences in WAXS and DSC profiles identify differences in the backsheet structure and design, which result in different mechanical, insulation, and durability characteristics.

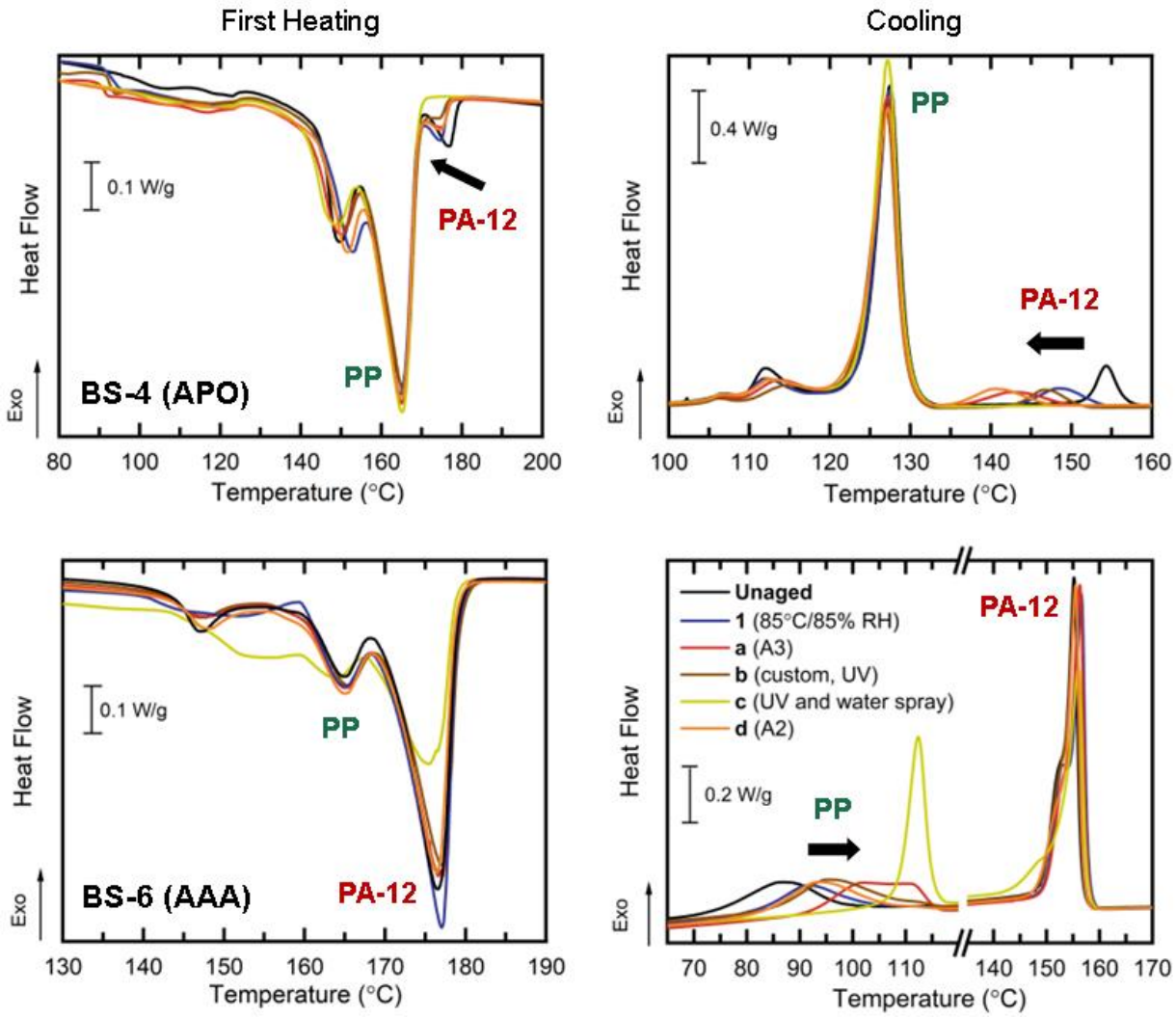

Fig. 6 DSC thermograms from first heating cycle (left) and cooling cycle (right) of PA- and PP-containing backsheets BS-4 (APO) and BS-6 (AAA) after 4000 h of UV weathering (tests a, b, c, and d) and hygrometric aging (test 1 (85°C/85% RH)).

Fig. 6 compares DSC first heating and cooling cycles of these two backsheets after various accelerated tests. DSC and WAXS confirmed that PA-12 is the dominant polymer (in terms of weight) in BS-6 (AAA), whereas PP is the dominant polymer in BS-4 (APO). These polymers constitute the core of the two backsheets, respectively. The steady PP DSC peaks with melting and crystallization temperatures for BS-4 (APO) of T_m ~ 164°C and T_c ~ 127°C, respectively, suggest that the PP core is negligibly affected by aging. In contrast, the PA-12 air side layer (T_m ~ 175°C, T_c ~ 154°C) degraded upon aging, and the corresponding DSC peaks exhibited shifts to lower temperatures. Shifts of the DSC crystallization peak were observed for all test conditions, but to the greatest extent in tests a (A3) and d (A2), which had the highest UV intensity (a shift of −13°C). The temperature during the photolytic test (55°C in d (A2) as opposed to 65°C in a (A3)) did not play a significant role in the PA degradation, confirming that UV is the primary driver of the PA degradation mechanism: UV-induced photo-oxidation associated with surface micro-cracking [4],[28]. The increase in the FTIR peak at 1735 cm^{-1} from the formation of imide groups can be observed in the FTIR spectra of BS-4 (APO) (Fig. 7b), consistent with previous studies [4].

In BS-6 (AAA), both PP and PA were affected by aging, mainly in test c (UV and water spray), followed by test a (A3). Chain scission of PP and an increase in crystallinity took place, evidenced by the shifts to higher temperature in the DSC cooling cycle. Temperature is the driving force for crystallization and embrittlement of PP, as evidenced by comparing tests a (A3) and d (A2), which applied 65°C and 55°C, respectively. This increase in crystallinity of the PP core came with a reduction of elongation to break (EtB) in AAA backsheets, ultimately leading to backsheet failure under mechanical loads [4],[9].

During test c (UV and water spray), the PA-12 DSC peaks gradually shifted, reduced in intensity, and finally disappeared in BS-4 (APO), suggesting material erosion or other significant changes in material crystallinity and molecular structure. PAs are vulnerable to both UV and moisture. Moisture changes molecular mobility, acting as plasticizer−reducing the elastic modulus and increasing elongation of the material [30]. However, at sufficiently high temperatures and moisture levels, PA can degrade by hydrolysis, similarly to PET [31],[32],[33]. To shed light on the complex behavior of PA-12 in BS-4 (APO) under UV and water spray in test c, Fig. 7 compares the DSC, FTIR, and surface morphology. DSC reveals progressive shifts to lower temperature and reduction of the PA peaks during heating and cooling cycles (Fig. 7a).

FTIR (Fig. 7b) detected the chemical signature of PA, confirming that the air side layer is still present after 4000 h of weathering with test c. However, chemical changes did take place. The increase in bands around 500 cm^{-1} suggests surface erosion and the presence of TiO_2 pigments on the surface. The increase in the peak at 1735 cm^{-1} corresponding to carbonyl (C=O) bond vibration of imide groups and the broadening of the hydroxyl (-OH) band at 3300 cm^{-1} suggest UV photo-oxidation. In test c, identical chemical groups were affected by aging than via photolytic tests a (A3) and d (A2), but to a lower extent (Fig. S6). This confirms that UV played only a partial role in the backsheet degradation mechanism in test c (UV and water spray). The region of spectra between 1250 and 900 cm^{-1} decreased instead of increasing as compared to the photolytic tests. Microscope images (Fig. 7c) of the aged surface show cracking and partial loss of material from the surface by abrasion from water spray. Micro-cracking and erosion were also observed on the air side layer of BS-6 (AAA) (Fig. S7). This demonstrates that the combination of stressors in test c (UV and water spray) has a significantly greater impact on the material degradation than the single stress UV or damp heat tests alone. Liquid water can transport the products of degradation off of the surface, including products that might remain and mask against subsequent damage.

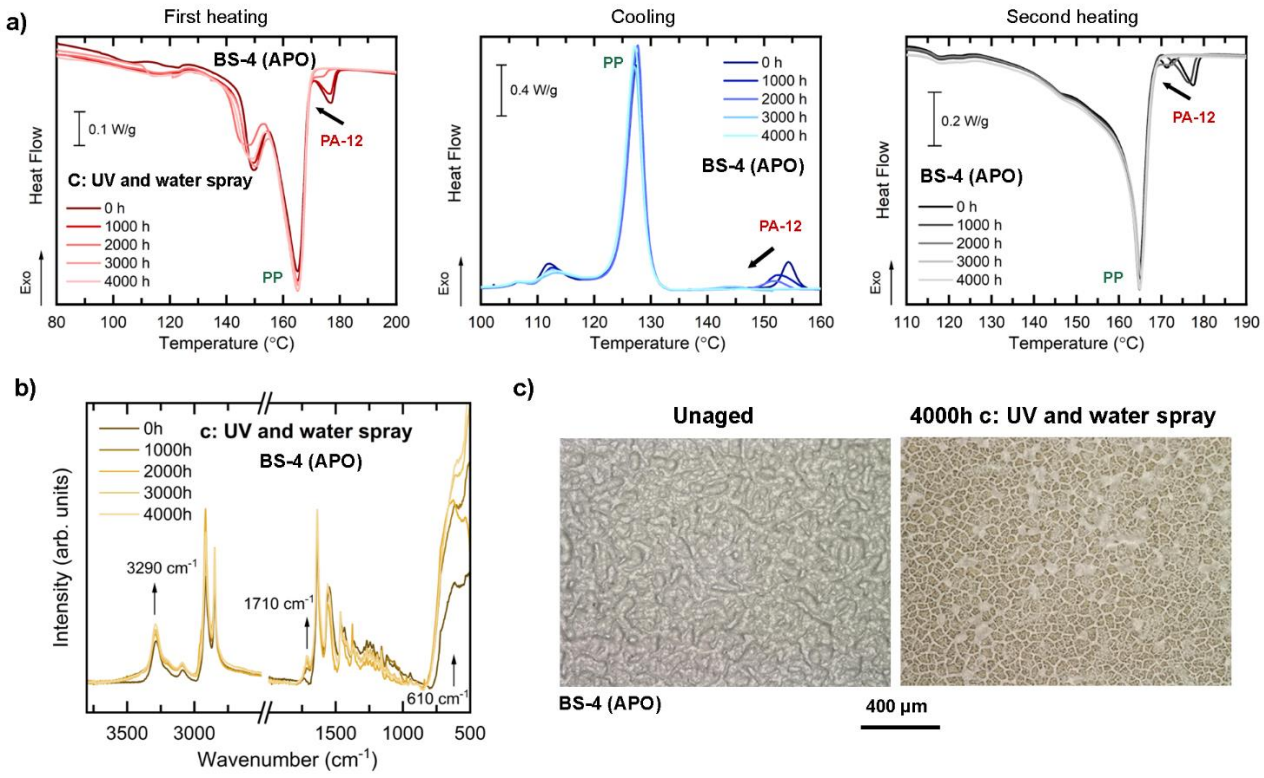

Fig. 7 BS-4 (APO) aged with test c (UV and water spray): (a) DSC of all backsheet layers, (b) FTIR-ATR spectra of the air side of the backsheet, and (c) microscope images of the PA outer (air side) surface. The arrows indicate changes in the peaks of interest.

BS-6 (AAA) is mechanically reinforced by randomly oriented glass fibers, and the unaged backsheet has the lowest elastic effective modulus and toughness of the backsheets in this study [5]. The complete loss of mechanical toughness was observed after only 1000 h of aging with all tests, confirming that BS-6 is vulnerable to both photolytic and hydrolytic degradation (Fig. S8). The identical loss of mechanical performance in this study for all photolytic and hygrometric aging tests suggests a loss of adhesion between the glass fibers and polymer matrix in the core, perhaps from a difficulty in manufacturing. Test c (UV and water spray) was the only test that caused substantial reduction in the ultimate tensile strength of greater than 50% as in UL 746B [34] (Fig. 8). Glass fibers were observed during microscope imaging of BS-6 (AAA) after test c, suggesting erosion of the PA air side surface layer (Fig. S7). The severity of test c can be clearly distinguished from the other tests.

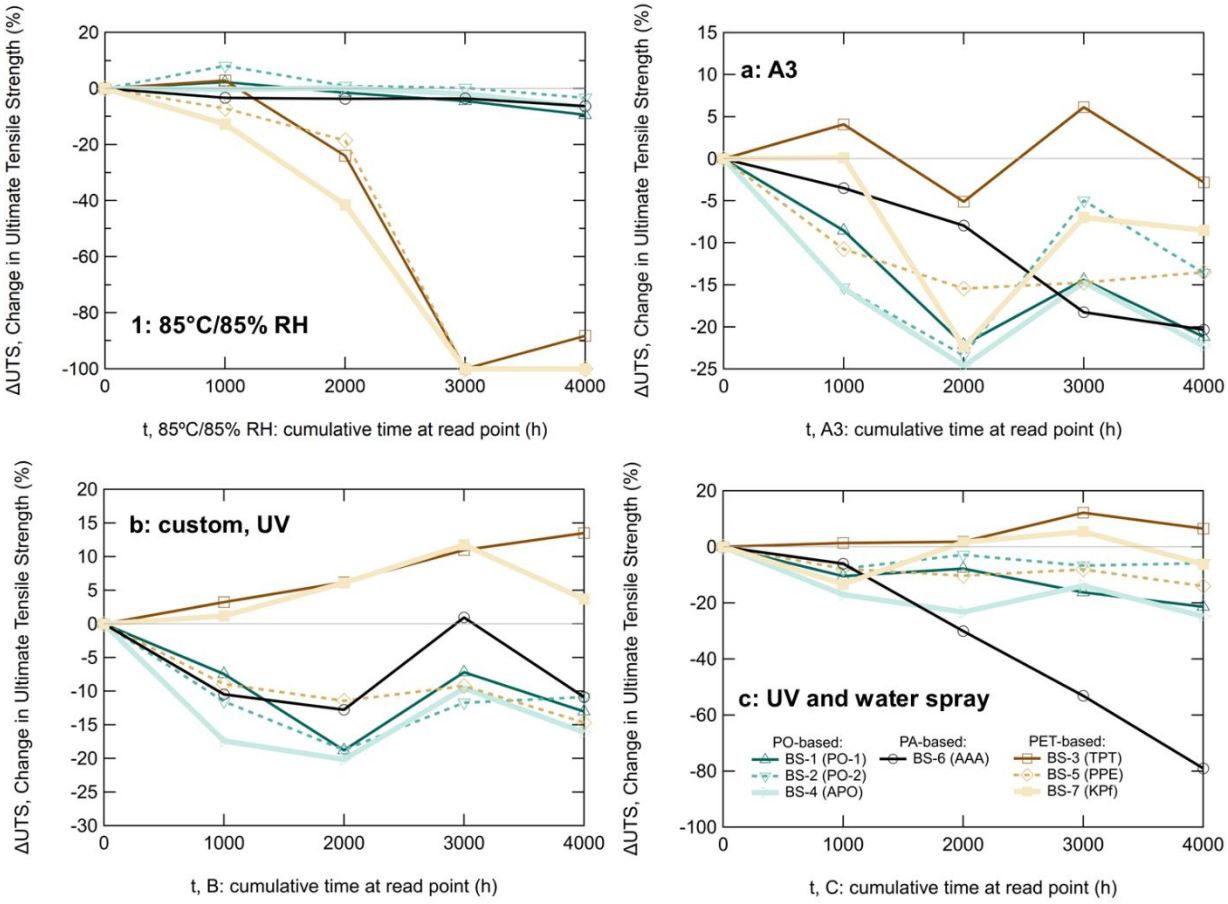

Fig. 8 Change in ultimate tensile strength of all seven backsheets after hygrometric tests 1 (85°C/85% RH), and photolytic tests a (A3), b (custom, UV), and c (UV and water spray) measured using tensile testing on five backsheet replicates in the transverse direction.

Fig. S9 shows an analysis of backsheets' insulation properties with aging, after the Weibull analysis of the breakdown voltage (V_{BD}) measured on six replicate backsheet specimens. While V_{BD} remained mostly above the threshold of the tester (100 kV) for PET-based backsheets for all aging conditions, BS-6 (AAA) was typically measured to be ~60 kV. Test c (UV and water spray) stood out in the breakdown voltage test, as all coextruded PO- and PA- based backsheets exhibited a linear decrease in the V_{BD}. All backsheets, including BS-6 (AAA), remained above the V_{BD} threshold of 8 kV, the safety requirement for a 1500V DC PV system in the IEC 61730-2 [15].

c) Polyolefin-based experimental coextruded backsheets

PO-based BS-1 (PO-1), BS-2 (PO-2), and BS-4 (APO) are coextruded backsheets consisting of a PP core layer and an LDPE sun side layer, but with different outer air-facing layers. The experimental BS-1 (PO-1) is entirely a PO backsheet, with the air side layer being PP, as in the core, but with a more robust formulation to protect the core from the environment. In the experimental BS-2 (PO-2), the air side layer is polybutylene terephthalate (PBT), and in the recently developed BS-4 (APO), the air side layer is PA-12.

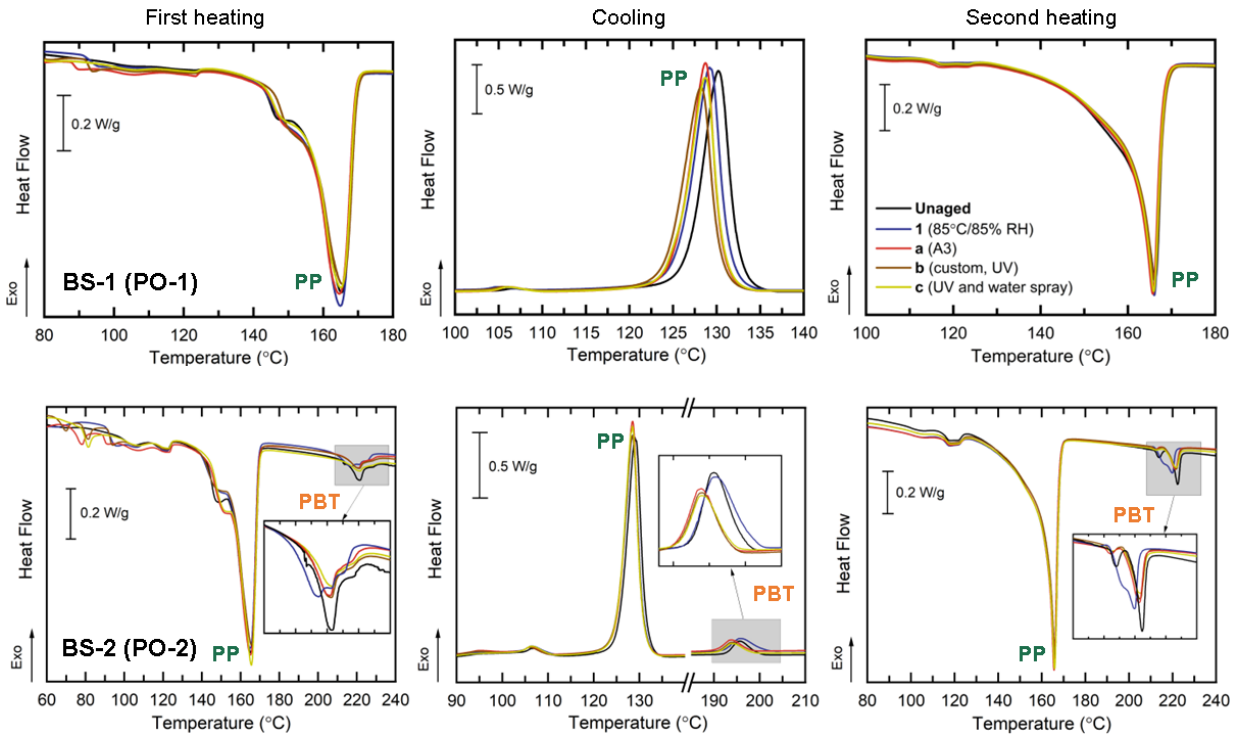

Fig. 9 DSC thermograms of PO-based, experimental, coextruded BS-1 (PO-1) and BS-2 (PO-2) comparing aging with hygrometric test 1 (85°C/85% RH) and photolytic tests a (A3), b (custom UV), and c (UV and water spray).

Fig. 9 summarizes the DSC profiles of BS-1 (PO-1) and BS-2 (PO-2) after 4000 h of various tests. The prominent melting peak at ~168°C corresponds to the melting of the PP in the core in BS-2 (PO-2) and the core and air side layers in BS-1 (PO-1). The small melting peak at ~120°C corresponds to melting of the LDPE sun side layer, and the melting peak at ~220°C in BS-2 (PO-2) corresponds to the PBT air side layer. The tightly overlapping PP peaks on the second DSC heating suggest that minimal irreversible damage of the PO-based core occurred during any of the aging tests. Shifts to lower temperatures of the PP crystallization peak near 130°C were observed during cooling of BS-1 (PO-1). The shifts of <4°C are likely related to the damage of the outer layer, as confirmed by FTIR in Fig. 10. These changes may result from chain scission reactions from UV and/or elevated temperatures, but these changes are much less significant than the hydrolytic damage to PET in commercial backsheets (DSC crystallization peak shifts >20°C) (Fig. 1 and Fig. 2) or to PP in BS-6 (AAA) (Fig. 6). In BS-2 (PO-2), the PBT air side layer was affected by aging, as evidenced by changes in the melting and crystallization peaks (T_m ~ 220°C and T_c ~ 195°C, respectively) in all three DSC cycles. Non-negligible changes were noted after aging with test 1 (85°C/85% RH), the temperature of this test being above the T_g of PBT (~60°C).

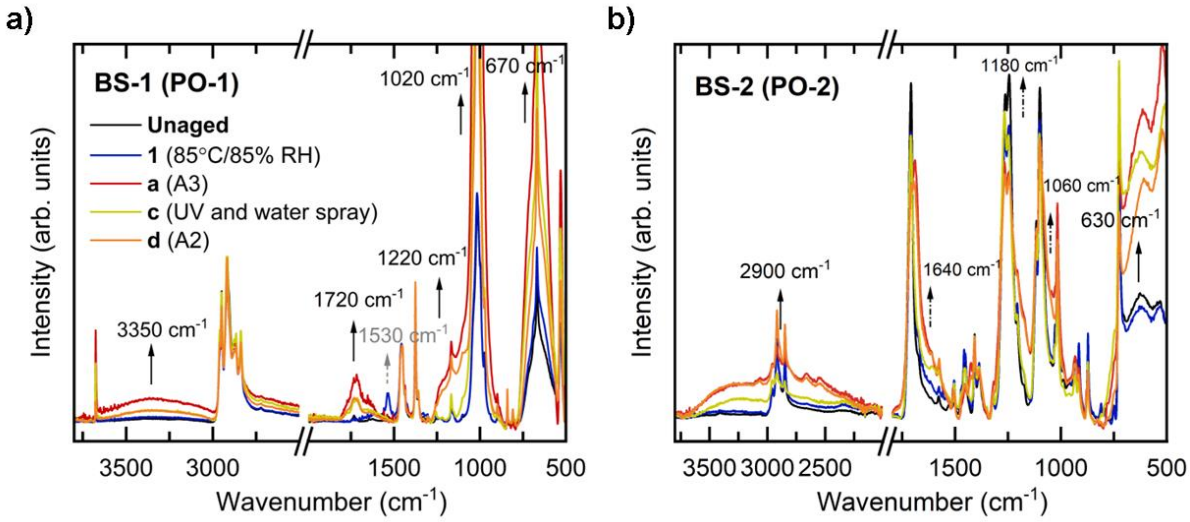

Fig. 10 FTIR-ATR spectra of the outer layer of (a) BS-1 (PO-1), and (b) BS-2 (PO-2) comparing unaged to aged (4000 h) backsheets from MiMos for tests 1 (85°C/85% RH), a (A3), c (UV and water spray), and d (A2).

The FTIR spectra of BS-1 (PO-1) and BS-2 (PO-2) outer layers in MiMos and coupons detected minor chemical changes after 4000 h of any of the hygrometric tests, with test 1 (85°C/85% RH) shown in Fig. 10. Both the a (A3) and c (UV and water spray) tests resulted in an increase in the shoulders centered around 1640 cm^{-1} (carbonyl C=O bonds) and broadening of the region centered at 2900 cm^{-1} (hydroxyl -OH stretch) in BS-2 (PO-2), similar to the UV-induced degradation of PET forming terephthalic acid described in Section 3 a) (Fig. S3) [16]. The increase in the 800–500-cm^{-1} region of spectra is associated with surface roughening exposing TiO_2 pigments. In BS-1 (PO-1), an increase in the bands around 1220 cm^{-1} (C-O stretch), 1720 cm^{-1} (C=O stretch), and 3350 cm^{-1} (-OH stretch) also suggests photo-oxidation and scission of the polymer chain. The greater extent of the surface damage in the dry photolytic tests a (A3), b (custom, UV), and d (A2) as compared to test c (UV and water spray) indicates that UV is the main stressor in dry conditions. In test c, the degradation products were likely removed by water spray, revealing fresh material from underneath, provided the UV damage was limited to outermost nanometers of the surface. Comparing tests a (A3) at 65°C and d (A2) at 55°C, the temperature difference appears to have a small impact on the backsheet degradation.

To understand how the chemical and crystalline changes affected the integrity of the air side backsheet layers, we imaged the outer surface. Fig. 11 shows the microscope images for the PO-based BS-1 (PO-1) (PP material), BS-2 (PO-2) (PBT), and BS-4 (APO) (PA-12) from the center of the MiMos. Despite surface chemical changes with UV weathering observed in the corresponding FTIR spectra (Fig. 10), no cracks were formed in the BS-1 (PO-1) or BS-2 (PO-2) MiMos (Fig. 11) or coupons (not shown). Cracks up to ~100 µm in length were observed on the air side layer of BS-4 (APO) after a (A3), b (custom, UV), and d (A2) tests, as discussed in Section 3 b) (Fig. S7). Macro-cracking of the PBT air side of BS-2 (PO-2) was observed after aging with test 1 (85°C/85% RH) (Fig. S10) and can be attributed to embrittlement from hydrolysis of PBT, a similar degradation mechanism affecting PET. Although no cracking was observed in the corresponding BS-2 (PO-2) coupon, localized cracking and loss of surface layer was observed after

aging of BS-5 (PPE) coupons and MiMos with test 1 (85°C/85% RH) [9]. An increase in surface roughness with material erosion was observed for test c (UV and water spray) in all backsheets.

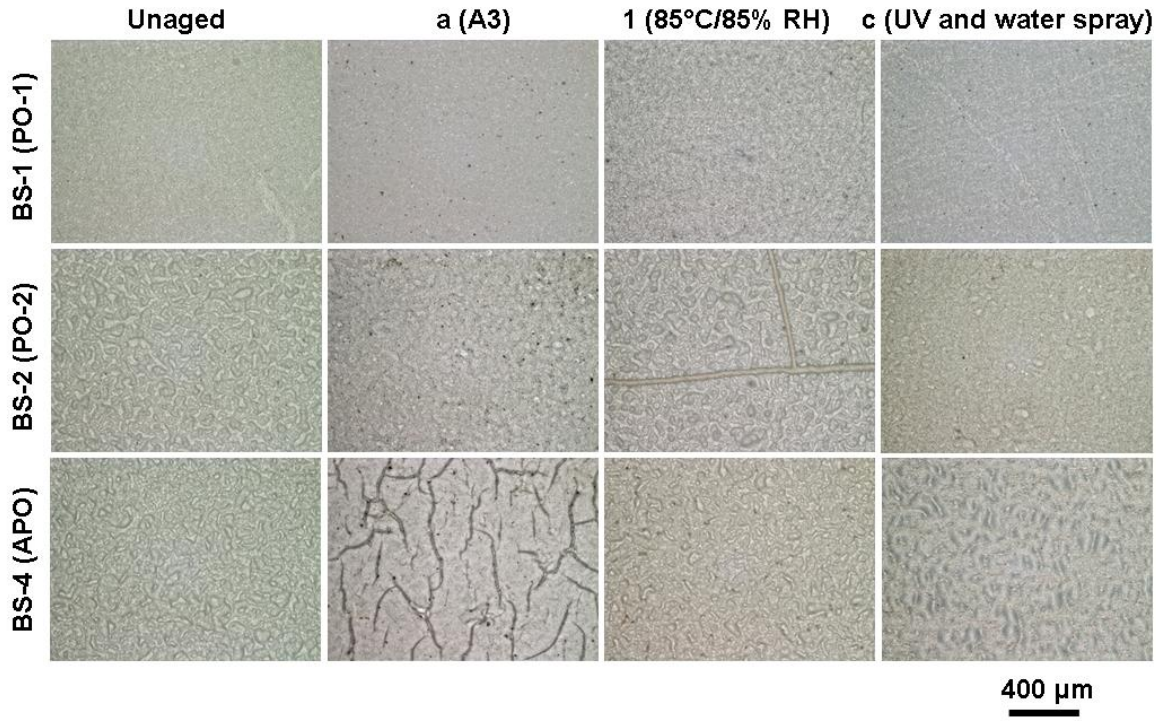

Fig. 11 Microscope images from the center of the MiMo air side surface of PO-based, coextruded fluoropolymer-free BS-1 (PO-1), BS-2 (PO-2), and BS-4 (APO) before and after 4000 h of tests a (A3), 1 (85°C/85% RH), and c (UV and water spray).

The mechanical properties of the backsheets were evaluated by tensile testing. In addition to ultimate tensile strength (UTS) (Fig. 8), characteristics including elastic modulus (E), yield stress (σ_y), elongation to break (EtB), and toughness (U) were extracted from stress-strain curves. These characteristics are discussed more in detail in Ref. [9]. Fig. 8 compares the UTS values for all backsheets for tests a (A3), b (custom, UV), c (UV and water spray) and 1 (85°C/85% RH). Catastrophic loss of UTS from the embrittlement of PET during test 1 (85°C/85% RH) was observed for all PET-based backsheets, with reduction in mechanical properties starting as early as 1000 h, followed by complete loss at 3000 h. The morphology of the fracture revealed a brittle fracture of the core into irregularly shaped pieces of different sizes after test 1 (85°C/85% RH), whereas a straight edge was observed in specimens unaged or following test a (A3) [9]. No drastic loss in UTS and embrittlement was observed for tests 2 (65°C/85% RH) (<25%) and 3 (45°C/85% RH) (<5%), or any of the photolytic (including custom) tests (Fig. 8 and Fig. S11).

Test c (UV and water spray) resulted in a gradual loss of UTS for BS-6 (AAA) (80% after 4000 h) (Fig. 8). This suggests creation of a surface defect population from erosion and/or corrosion of the glass fibers in the core of BS-6 (AAA). Fig. S8 compares the toughness of PA-based BS-6 (AAA), PO-based BS-1 (PO-1), and PET-based BS-3 (TPT). A nearly complete loss of toughness of BS-6 (AAA) was observed after 1000 h for all UV weathering and hygrometric tests. A reduction in UTS and toughness in PET-based backsheets results from hydrolysis and embrittlement of the backsheet core, which dominates the

mechanical response of BS-3 (TPT), BS-5 (PPE), and BS-7 (KPf). Mass transport of water through the air-facing layer could compromise the PET core.

For PO-based backsheets, a relatively small reduction in UTS was observed in all tests, suggesting that the backsheet core retained most of its mechanical integrity despite the modest surface damage observed in microscopy and FTIR spectroscopy. Only the BS-4 (APO) showed a greater loss of mechanical toughness at select read points during UV weathering. The stochastic nature of damage, rather than a clear trend with UV dose, suggests surface damage rather than accumulating degradation of the core. The local UV-induced degradation of the PA air side layer observed in FTIR, DSC, and microscopy likely makes the backsheet core more vulnerable to weathering in the exposed areas. While all the PO-based specimens demonstrated a significant inelastic deformation on breaking, for BS-2 (PO-2) and BS-4 (APO), the micro-scale fractography revealed a surface morphology that depends on specimen aging history, suggesting a complexity for the degradation mechanism(s) that depends on the stressors during aging [9].

4/ Discussion:

a) Surface vs. core degradation and material selection

This study revealed two types of backsheet degradation modes, surface and core damage, which have different impacts on backsheet properties and their durability. Surface degradation was often observed after photolytic aging caused by UV photo-oxidation of the air side layer. FTIR analysis revealed that degradation by UV photo-oxidation occurred to some extent on all seven backsheets, regardless of the polymeric material constituting the air side layer and its additive formulation. Change in gloss, which varied with UV weathering, suggested surface roughening [9]. Polymers in backsheets are typically not pure; instead, they are often blended with other polymers and additives, including UV absorbers, stabilizers, antioxidants, and pigments, all of which affect environmental robustness. For BS-4 (APO) and BS-6 (AAA), both of which contain an outer (air side) PA-12 layer, UV weathering resulted in surface cracking. No cracking was observed on the air-facing surface of any other backsheets. In all seven backsheets, test c (UV and water spray) resulted in surface erosion. The water spray is suspected to cause material transport (i.e., loss of degradation products) that is not representative of the PV application. This is further supported by observations of interior glass fibers in the microscope images of BS-6, as opposed to a partial removal of the outer layer through chalking of the surface in fielded AAA backsheets [4],[28]. Absorption of light by additives (TiO_2, UV absorbers) and chromophore species typically ensures that UV degradation is limited to the outermost micrometers of the surface that protects the core layer. The core effectively governs mechanical and electrical properties of the backsheet. However, in BS-4 (APO), surface cracking either generated sufficiently sized defects or locally exposed the core layer, compromising, to a varied extent, the mechanical properties (e.g., toughness) of the backsheet. BS-6 (AAA) showed signs of both surface and core degradation, leading to a complete loss of mechanical properties. Its constituent materials, PA-12 and PP, are both inherently vulnerable to UV, thermal, and hydrolytic degradation. Elevated temperatures caused thermal degradation of the PP in the core, moisture initiated hydrolytic degradation of the PA, and loss of adhesion between the glass fibers and the polymer matrix in the core resulted in inferior durability compared to all other backsheets. Despite similarities in the polymeric materials used in both BS-6 (AAA) and BS-4 (APO), this study demonstrates that the backsheet design and formulation of constituent layers greatly affect durability.

While surface degradation is the dominant degradation mode in PO-based backsheets, hydrolysis of the core prevails in PET-based backsheets under high-temperature and high-humidity conditions.

Hydrolytic degradation of PET caused embrittlement and loss of mechanical performance early in test 1 (85°C/85% RH). Catastrophic hydrolysis was not observed in lower temperature hygrometric tests, as the toughness and strength of BS-3 (TPT), BS-5 (PPE), and BS-7 (KPf) was not reduced by more than 50% from aging with tests 2 (65°C/85% RH) or 3 (45°C/85% RH) (Fig. S11). Below the T_g of PET (~80°C), hydrolysis is limited. However, above T_g, hydrolysis occurs readily with acceleration from both temperature and RH, consistent with its highly thermally activated nature (with an activation energy of 129 $kJ \cdot mol^{-1}$) [35]. Chain scission reactions cause recrystallization of the polymer, leading to a greater degree of crystallinity and embrittlement of the backsheet core. Because polymers are inherently permeable to water, the choice of the protective outer layer had minimal effect on the backsheet durability, and all three studied PET-based backsheets performed similarly in tensile testing. While 85°C/85% RH is commonly used in aging studies of PV materials, the absolute humidity of 298 g/m^3 far exceeds the world record of 40 g/m^3 [36] or the typical PV application [20]. The air side layers of BS-5 (PPE) and BS-2 (PO-2) are PET and PBT, respectively. These polymers have a similar molecular structure and exhibit chemical changes of similar nature after UV weathering. The T_g of both polymers is below 85°C, and consequently, these outer layers were shown to be vulnerable to hydrolysis in test 1 (85°C/85% RH), which manifested in the form of cracking and delamination in the corresponding MiMos.

b) Modified/custom vs. standard tests

Tests 1 (85°C/85% RH), a (A3), and c (UV and water spray) gave the greatest insight into backsheet durability, uncovering material susceptibilities to hydrolytic degradation in the dark (test 1), under UV weathering (test a), and with a combination of UV and water spray (test c). Test 1 (85°C/85% RH) revealed the weaknesses of PET-based backsheets to hydrolytic degradation of the core layer, which resulted in catastrophic failure. Whether this degradation mode is field relevant is a subject of debate; because module temperatures can reach as high as 80°C (the T_g of PET), but the absolute humidity to fuel hydrolysis at this temperature is not achieved for PV on Earth [37]. For moderate climates, the legacy PET-based backsheets, such as BS-3 (TPT), have proven capable of performing for modules now more than 30 years old [38]. Test conditions 2 (65°C/85% RH) and 3 (45°C/85% RH), which applied temperatures below the T_g of PET and below where the activation energy for hydrolysis becomes impactful, did not result in significant embrittlement of PET-based backsheets. None of the damp heat tests resulted in chemical changes at the backsheet surface or surface cracking. 1000 h of 85°C/85% RH is used in the IEC 61730-2 module safety and IEC 61215 module design type qualification [15],[11], while lesser temperature and humidity test conditions are not typically used in practice.

Out of the photolytic tests, test a (IEC method A3), with a UV intensity of 0.8 Wm^{-2} and a chamber temperature of 65°C, resulted in the greatest UV-induced photo-oxidation damage at the backsheet surface, closely followed by test d (A2), with the same UV intensity but a lower chamber temperature of 55°C. Chemical changes from the UV degradation observed in FTIR were comparable between tests a (A3) and d (A2); however, the higher temperature in test a (A3) resulted in an increased rate of polymer crystallization initiated by chain scission from photo-oxidation. This is particularly evident in the DSC of the sun side layer of BS-5 (PPE) and the air side layer of BS-7 (KPf), which were observed to form cracks in this study (BS-5 (PPE)) and in the field (BS-7 (KPf)) [22],[23] as a result of UV and elevated temperatures. Based on the FTIR surface analysis, test b (custom, UV), with a lower UV intensity of 0.55 Wm^{-2} and a comparable chamber temperature to tests a (A3) and d (A2), resulted in a lesser but still significant degree of UV degradation compared to the standard tests a (A3) and d (A2). Even though UV affects only the outermost micrometers of the backsheet air side layer surface, in selected materials, such as PAs, UV

damage can result in air side layer cracking exposing the more vulnerable core to the environment. Therefore, the UV tests are of great importance in backsheet testing to screen for embrittlement and surface erosion. The selection of greater chamber temperatures may be of interest for hot climates. For backsheets that are transparent to accommodate bifacial PV cells, UV weathering may also be used to verify the optical durability—because polymers often discolor and become less transmitting. The UV preconditioning test in the IEC 61730-2 module safety and IEC 61215 module design type qualification is roughly equal to 40 days equivalent field dose [15],[11], whereas the higher fidelity A3 weathering now applied in the IEC 62788-series standards gives ~5 years equivalent field dose [39].

Test c (UV and water spray) revealed additional degradation mechanisms not observed in the separate photolytic and hygrometric tests. Despite having the same UV intensity and temperature as test b (custom, UV), the FTIR spectra for test c suggested that the UV-induced damage to the surface was lesser compared to the dry tests (Fig. 10, Fig. S3, Fig. S5, and Fig. S6). Change in surface morphology in microscopy and surface roughness in gloss measurements [9] indicated that the water spray resulted in spalling and loss of surface material on all seven backsheets, which may be why the degradation from UV appears less significant in FTIR characterization—because fresh material was exposed. Test c resulted in partial layer loss observed on microscope images, and it was enhanced in backsheets showing cracking from UV (i.e., LDPE in BS-5 (PPE), PA-12 in BS-4 (APO) and BS-6 (AAA)). Water may also quench free radicals, inhibiting the sequence of chemical reactions for photo-oxidative degradation in some materials. The stressors of UV and water spray resulted in new degradation pathways in some backsheets, for example, BS-4 (APO) and BS-6 (AAA), where the PA-12 and PP materials changed crystalline properties. Test c caused the greatest decline in mechanical and insulating properties in the majority of backsheets, in particular BS-6 (AAA) and BS-4 (APO). This test is not likely to be field relevant, as there is no data on substantive erosion of backsheets in PV systems, including loss of the air side layer. Furthermore, the backs of modules typically do not directly face precipitation; rather, the PV backsheet is shielded from liquid water by the sun side of the module. However, this study demonstrates the impact of combining stressors into a single test to screen material vulnerabilities otherwise undetected by single stress tests, as advocated in recent studies [23],[40]. The screening for degradation modes in any accelerated test, however, always remains to be verified as field relevant.

c) Summary table

Table III: Summary of the degradation modes observed for different backsheets and accelerated stress tests.

<table>
<tr><th></th><th colspan="3">PET-based</th><th colspan="3">PO-based</th><th>PA-based</th></tr>
<tr><th></th><th>BS-3</th><th>BS-5</th><th>BS-7</th><th>BS-1</th><th>BS-2</th><th>BS-4</th><th>BS-6</th></tr>
<tr><td rowspan="4">Photolytic</td><td colspan="7">Surface UV photo-oxidation</td></tr>
<tr><td rowspan="3">Air side PVF structural degradation</td><td rowspan="3">Increase in crystallinity and cracking of LDPE sun side layer</td><td rowspan="3">Increase in air side PVDF crystallinity</td><td rowspan="3"></td><td rowspan="3"></td><td rowspan="3">PA-12 air side layer cracking</td><td>PA-12 air side layer cracking</td></tr>
<tr><td>Thermal degradation of PP core</td></tr>
<tr><td>Loss of backsheet toughness</td></tr>
<tr><td></td><td colspan="3">Hydrolysis and embrittlement of PET core, test 1 (85°C/85% RH)</td><td></td><td>Hydrolytic degradation</td><td>Signs of hydrolytic</td><td>Increase in crystallinity</td></tr>
</table>

<table>
<tr><td rowspan="4">Hygrometric</td><td colspan="3"></td><td rowspan="4"></td><td rowspan="4">of PBT air side resulting in macro-cracking in MiMos, test 1 (85°C/85% RH)</td><td rowspan="4">and/or thermal degradation of PA-12 air side, test 1 (85°C/85% RH)</td><td>of PA-12 and air side surface micro-cracking from hydrolytic and/or thermal degradation, test 1 (85°C/85% RH)</td></tr>
<tr><td colspan="3">Loss of backsheet mechanical properties from embrittlement, test 1 (85°C/85% RH)</td><td rowspan="3">Catastrophic loss of backsheet toughness after 1000h in all tests</td></tr>
<tr><td></td><td>Hydrolytic degradation of PET air side causing cracking in MiMos and coupons, test 1 (85°C/85% RH)</td><td>Increase in air side PVDF crystallinity, test 1 (85°C/85% RH)</td></tr>
<tr><td colspan="3"></td></tr>
<tr><td rowspan="5">Custom test c (UV and water spray)</td><td colspan="6">Surface erosion masking UV photo-oxidation</td></tr>
<tr><td rowspan="4"></td><td rowspan="4">Increase in crystallinity, cracking, and erosion of sun side LDPE</td><td rowspan="4">Increase in air side PVDF crystallinity</td><td rowspan="3"></td><td rowspan="3"></td><td>Cracking and removal of the air side PA-12 layer</td><td>Cracking and removal of the air side PA-12 layer</td></tr>
<tr><td rowspan="2">Structural changes in PA-12 air side layer</td><td>Degradation of all backsheet materials (PA-12, PP, glass fiber interface)</td></tr>
<tr><td>Loss of backsheet mechanical properties</td></tr>
<tr><td colspan="4">Reduced backsheet breakdown voltage</td></tr>
</table>

Conclusions:

This study compared changes in material properties to distinguish the enabling degradation mechanisms for seven PV backsheets through a variety of indoor accelerated stress tests. Multilayer backsheets were compared here in a third-party examination of the feasibility of novel materials, where the durability ultimately depends on both their proprietary additives and their manufacturing processes. A summary of these observations can be found in Table III.

Catastrophic embrittlement of the core layer in commercial laminated PET-based backsheets was observed for hygrometric aging at 85°C/85% RH. The elevated test temperature within the range of the

activation energy of PET and above its T_g triggered hydrolysis of the polymer, resulting in a complete loss of mechanical properties after 3000 h of aging. However, the 85°C/85% RH test is unlikely to be field relevant.

UV photo-oxidation of the outer (air side) surface layer took place in all backsheets, regardless of the polymer material and its additive formulation. However, in backsheets containing PA-12 air side layer, chemical changes resulted in surface cracking, partially exposing the core layer. UV and elevated temperatures can increase the crystallinity in polymers such as PVDF or LDPE, where the corresponding embrittlement leads to cracking under mechanical stress. Cracking of sun side LDPE was observed in the backsheet coupons, but this failure mode may be less relevant in the modules, where this layer is protected from UV by the module components, which also provide mechanical strain relief. Comparing the environmentally vulnerable BS-6 (AAA) with an experimental BS-4 (APO), it was shown that two backsheets with the same base materials (e.g., PA-12 and PP) can differ in durability depending on backsheet design and additives. This suggests that although PA-12 has weaknesses, the failures observed for AAA backsheets may not occur in all PA-based backsheets.

UV tests in dry conditions resulted in more UV photo-oxidation damage on the backsheet surface than a wet UV test, but this is likely related to the surface erosion from the water spray during aging (revealing fresher surface material) rather than quenching of free radicals by water during weathering. Application of custom test c, combining UV and water spray, resulted in new degradation mechanisms and surface erosion, showing once more the significance of combining stress factors into a single test.

PO-based experimental backsheet BS-1 (PO-1) proved to be a robust, fluoropolymer-free backsheet that retained its mechanical integrity throughout all tests, even test 1 (85°C/85% RH) where the industry-benchmark BS-3 (TPT) failed. Commercial PET-based backsheets provided the best electrical insulation properties throughout all tests, including the custom test c with UV and water spray, which compromised the properties of backsheets containing PP as core layer. Neither test 1 (85°C/85% RH) nor test c (UV and water spray) is expected to be field relevant. Overall, UV photo-oxidation causing surface damage was observed to be the dominant and most field valid degradation mode affecting all backsheets. However, it did not seem to transfer to the backsheet core, except through cracking of the air side layer in PA-12-containing backsheets BS-4 and BS-6. This study shows that with material and design engineering and optimization, coextruded experimental PO-based backsheets can be a durable alternative to commercial PET-based PV backsheets warranting further development and field validation.

Acknowledgements:

The authors would like to acknowledge Stephanie L. Moffitt for her contributions to the initial data collection; Elizabeth C. Palmiotti for leading the outdoor study and ongoing cross-sectional characterization of identical backsheet samples; and "Comparison of market-benchmark BACKsheet technologies to novel non-FLuoro-based coextruded materials and their correlation and ImPact on PV module degradation rates" (BACKFLIP) study contributors Kurt van Durme, Nicoleta Voicu, Milica Mrcarica, Frederic Dross, Nicola Sicchieri, Robert Janssen, and Sven Kreisig from Endurans Solar (formerly DSM) for their contributions to the project and data analysis. Funding was provided as part of the Durable Module Materials Consortium (DuraMAT), funded under Agreement 32509 by the U.S. Department of Energy (DOE), Office of Energy Efficiency and Renewable Energy (EERE) and Solar Energy Technologies

Office (SETO). This work was authored in part by the National Renewable Energy Laboratory, operated by Alliance for Sustainable Energy, LLC, for the U.S. DOE under contract no. DE-AC36-08GO28308. Use of the Stanford Synchrotron Radiation Lightsource, SLAC National Accelerator Laboratory, was supported by the U.S. DOE, Office of Basic Energy Sciences under Contract No. DE-AC02-76SF00515. The views expressed in the article do not necessarily represent the views of the DOE or the U.S. Government. The U.S. Government retains and the publisher, by accepting the article for publication, acknowledges that the U.S. Government retains a nonexclusive, paid-up, irrevocable, worldwide license to publish or reproduce the published form of this work, or allow others to do so, for U.S. Government purposes.

Data Availability

The datasets generated and/or analyzed during the current study are available in the DuraMAT Datahub, https://datahub.duramat.org/.

References:

[1] S. K. Chunduri and M. Schmela, "Market Survey: Backsheets & Encapsulation 2022 – 2023," 2023. [Online]. Available: https://taiyangnews.info/reports/taiyangnews-solar-module-innovations/

[2] V. Aryan, M. Font-Brucart, and D. Maga, "A comparative life cycle assessment of end-of-life treatment pathways for photovoltaic backsheets," *Prog. Photovoltaics Res. Appl.*, vol. 26, no. 7, pp. 443–459, 2018, doi: 10.1002/pip.3003.

[3] P. de Wild, M. de Wild-Scholten, and I. Goudswaard, "Life cycle assessment of photovoltaic module backsheets," *Prog. Photovoltaics Res. Appl.*, pp. 1–13, 2023, doi: 10.1002/pip.3755.

[4] M. Owen-Bellini *et al.*, "Towards validation of combined-accelerated stress testing through failure analysis of polyamide-based photovoltaic backsheets," *Sci. Rep.*, vol. 11, no. 2019, pp. 1–13, 2021, doi: 10.1038/s41598-021-81381-7.

[5] M. Thuis *et al.*, "A Comparison of Emerging Nonfluoropolymer-Based Coextruded PV Backsheets to Industry-Benchmark Technologies," *IEEE J. Photovoltaics*, vol. 12, no. 1, pp. 88–96, 2022, doi: 10.1109/JPHOTOV.2021.3117915.

[6] M. Kottek, J. Grieser, C. Beck, B. Rudolf, and F. Rubel, "World map of the Köppen-Geiger climate classification updated," *Meteorol. Zeitschrift*, vol. 15, no. 3, pp. 259–263, 2006, doi: 10.1127/0941-2948/2006/0130.

[7] E. C. Palmiotti, B. H. King, R. L. Arnold, S. Uličná, and D. C. Miller, "A comparison of emerging photovoltaic backsheets between outdoor locations," *2023 IEEE 50th Photovolt. Spec. Conf.*, 2023.

[8] S. Ulicna *et al.*, "BACKFLIP: Identification of Materials and Changes upon Aging of Emerging Fluoropolymer-Free and Industry-Benchmark PV Backsheets," *2021 IEEE 48th Photovolt. Spec. Conf.*, no. 32509, pp. 1842–1847, 2021, doi: 10.1109/PVSC43889.2021.9518781.

[9] N. M. Al Hasan *et al.*, "BACKFLIP: A Comparison of Market-Benchmark Backsheet Technologies to Novel Non-Fluoro-Based Coextruded Materials and Their Correlation and Impact on PV Module Degradation Rates: Final Results of the Study at 4000 Hours or 2 Years," *NREL-SR-5K00-80606*, pp. 1–106, 2023.

[10] IEC TS 62788-7-2, "Measurement procedures for mateials used in photovoltaic modules - Part 7-

2: Environmental exposures - Accelerated weathering tests of polymeric materials," *Int. Electrotech. Comm.*, pp. 1–26, 2017.

[11] IEC 61215-2, "Crystalline Silicon Terrestrial Photovoltaic (PV) Modules—Design Qualification and Type Approval- Part 2: Test procedures," *Int. Electrotech. Comm. Geneva*, pp. 1–97, 2016.

[12] P. Y. Yuen, S. L. Moffitt, F. D. Novoa, L. T. Schelhas, and R. H. Dauskardt, "Tearing and reliability of photovoltaic module backsheets," *Prog. Photovoltaics Res. Appl.*, vol. 27, no. 8, pp. 693–705, 2019, doi: 10.1002/pip.3144.

[13] B. H. Toby and R. B. Von Dreele, "GSAS-II: the genesis of a modern open-source all purpose crystallography software package," *J. Appl. Crystallogr.*, vol. 46, no. 2, pp. 544–549, 2013, doi: 10.1107/S0021889813003531.

[14] IEC TS 62788-2, "Measurement procedures for mateials used in photovoltaic modules - Part 2: Polymeric materials used for frontsheets and backsheets," *Int. Electrotech. Comm. Geneva*, pp. 1–88, 2017.

[15] IEC 61730-2, "Photovoltaic (PV) module safety qualification - Part 2: Requirements for testing," *Int. Electrotech. Comm.*, 2023.

[16] T. Sang, C. J. Wallis, G. Hill, and G. J. P. Britovsek, "Polyethylene terephthalate degradation under natural and accelerated weathering conditions," *Eur. Polym. J.*, vol. 136, p. 109873, 2020, doi: 10.1016/j.eurpolymj.2020.109873.

[17] N. S. Allen, M. Edge, M. Mohammadian, and K. Jones, "Physicochemical aspects of the environmental degradation of poly(ethylene terephthalate)," *Polym. Degrad. Stab.*, vol. 43, no. 2, pp. 229–237, 1994, doi: 10.1016/0141-3910(94)90074-4.

[18] C. Sammon, J. Yarwood, and N. Everall, "FT-IR study of the effect of hydrolytic degradation on the structure of thin PET films," *Polym. Degrad. Stab.*, vol. 67, no. 1, pp. 149–158, 2000, doi: 10.1016/S0141-3910(99)00104-4.

[19] A. Ballara and J. Verdu, "Physical aspects of the hydrolysis of polyethylene terephthalate," *Polym. Degrad. Stab.*, vol. 26, no. 4, pp. 361–374, 1989, doi: 10.1016/0141-3910(89)90114-6.

[20] M. D. Kempe and J. H. Wohlgemuth, "Evaluation of temperature and humidity on PV module component degradation," *Conf. Rec. IEEE Photovolt. Spec. Conf.*, pp. 120–125, 2013, doi: 10.1109/PVSC.2013.6744112.

[21] F. B. Marcotte, J. A. Campbell, J. A. Cleavland, and D. T. Turner, "Photolysis of Poly(ethylene Terephthalate)," *J. Polym. Sci. Part A Polym. Chem.*, vol. 5, pp. 481–501, 1967, doi: 10.1002/pol.1967.150050308.

[22] DuPont, "DuPont global PV reliability: 2020 Field analysis," 2020. [Online]. Available: https://skypower.com/wp-content/uploads/2020/08/Global-Field-Reliability-Report-2020.pdf

[23] S. Uličná *et al.*, "A study of degradation mechanisms in PVDF-based photovoltaic backsheets," *Sci. Rep.*, vol. 12, no. 1, pp. 1–11, 2022, doi: 10.1038/s41598-022-18477-1.

[24] S. L. Moffitt *et al.*, "Microstructure changes during failure of PVDF-based photovoltaic backsheets," *Prog. Photovoltaics Res. Appl.*, vol. 31, no. 1, pp. 26–35, 2023, doi: 10.1002/pip.3605.

[25] S. Therias, G. Rapp, C. Masson, and J. L. Gardette, “Limits of UV-light acceleration on the photooxidation of low-density polyethylene,” *Polym. Degrad. Stab.*, vol. 183, p. 109443, 2021, doi: 10.1016/j.polymdegradstab.2020.109443.

[26] M. Bertoldo, S. Bronco, C. Cappelli, T. Gragnoli, and L. Andreotti, “Combining Theory and Experiment to Study the Photooxidation of Polyethylene and Polypropylene,” *J. Phys. Chem. B*, vol. 107, no. 43, pp. 11880–11888, 2003, doi: 10.1021/jp035427h.

[27] S. Ulicna *et al.*, “Failure Analysis of a New Polyamide-Based Fluoropolymer-Free Backsheet after Combined-Accelerated Stress Testing,” *IEEE J. Photovoltaics*, vol. 11, no. 5, pp. 1197–1205, 2021, doi: 10.1109/JPHOTOV.2021.3090152.

[28] G. C. Eder *et al.*, “Error analysis of aged modules with cracked polyamide backsheets,” *Sol. Energy Mater. Sol. Cells*, vol. 203, p. 110194, 2019, doi: 10.1016/j.solmat.2019.110194.

[29] P. Gebhardt, L. P. Bauermann, and D. Philipp, “Backsheet Chalking - Theoretical background and relation to backsheet cracking and insulation failures,” *35th Eur. Photovolt. Sol. Energy Conf. Exhib.*, 2018.

[30] T. S. Ellis, “Moisture-induced plasticization of amorphous polyamides and their blends,” *J. Appl. Polym. Sci.*, vol. 36, no. 3, pp. 451–466, 1988, doi: 10.1002/app.1988.070360301.

[31] B. Jacques, M. Werth, I. Merdas, F. Thominette, and J. Verdu, “Hydrolytic ageing of polyamide 11. 1. Hydrolysis kinetics in water,” *Polymer (Guildf).*, vol. 43, no. 24, pp. 6439–6447, 2002, doi: 10.1016/S0032-3861(02)00583-9.

[32] N. Chaupart, G. Serpe, and J. Verdu, “Molecular weight distribution and mass changes during polyamide hydrolysis,” *Polymer (Guildf).*, vol. 39, no. 6–7, pp. 1375–1380, 1998, doi: 10.1016/S0032-3861(97)00414-X.

[33] A. Touris *et al.*, “Effect of molecular weight and hydration on the tensile properties of polyamide 12,” *Results Mater.*, vol. 8, p. 100149, 2020, doi: 10.1016/j.rinma.2020.100149.

[34] UL Standard, “UL 746B: Polymeric Materials – Long Term Property Evaluations,” 2018

[35] J. E. Pickett and D. J. Coyle, “Hydrolysis kinetics of condensation polymers under humidity aging conditions,” *Polym. Degrad. Stab.*, vol. 98, no. 7, pp. 1311–1320, 2013, doi: 10.1016/j.polymdegradstab.2013.04.001.

[36] Guinness World Records, “Highest dewpoint temperature.” https://www.guinnessworldrecords.com/world-records/645732-highest-dewpoint-temperature (accessed Jan. 01, 2024).

[37] IEC 60721-2-1:2013, “Classification of environmental conditions - Part 2-1: Environmental conditions appearing in nature - Temperature and humidity,” *Int. Electrotech. Comm.*, pp. 1–21, 2013.

[38] Z. Liu *et al.*, “Quantitative analysis of degradation mechanisms in 30-year-old PV modules,” *Sol. Energy Mater. Sol. Cells*, vol. 200, p. 110019, 2019, doi: 10.1016/j.solmat.2019.110019.

[39] J. Morse, M. Thuis, D. Holsapple, R. Willis, M. D. Kempe, and D. C. Miller, “Degradation in photovoltaic encapsulant transmittance: Results of the second PVQAT TG5 artificial weathering study,” *Prog. Photovoltaics Res. Appl.*, vol. 30, no. 7, pp. 763–783, 2022, doi: 10.1002/pip.3551.

[40] M. Owen-Bellini *et al.*, “Advancing reliability assessments of photovoltaic modules and materials using combined-accelerated stress testing,” *Prog. Photovoltaics Res. Appl.*, vol. 29, no. 1, pp. 64–82, 2021, doi: 10.1002/pip.3342.